Methods of Electron Structure Spectroscopy in Molecular Organic Solids Based on Space Charge Conductivity

F. SCHAUER, R. NOVOTNÝ, and V. ČECH

Faculty of Chemistry, Technical University, CZ-637 00 Brno

Received 18 April 1996

Space-charge-limited currents (SCLC) in steady state (S-SCLC) may be with advantage used as tools for the study of the density of localized states (DOS) in disordered inorganic and organic semiconductors. S-SCLC are observed with advantage in high resistivity materials with mobile carriers.

In this paper the S-SCLC method is presented, focusing on the DOS evaluation, steady-state drift mobility, temperature dependence of S-SCLC and the statistical shift of the Fermi level in S-SCLC, SCLC in organic materials with amphoteric defects and contact limitations as a result of detailed modelling of real structures exhibiting SCLC. Paper may serve as a review of the present state of the space-charge-limited currents theory.

Steady-state space-charge-limited currents (S-SCLC) [1], though discovered for the branch of amorphous semiconductors [2], have been used as a simple method for the density-of-states (DOS) study [3—6]. Less followed were the potential possibilities to address the temperature-dependent SCLC and concomitant Meyer—Neldel rule, the mobility issue, the contact ideality, and sample homogeneity [7—9].

Physical Background

Basically, depending on the relation of the transit time t_t and the Maxwell relaxation time t^M, three regimes of transport, summarized in the table, may be observed.

1	$t^M < t_t$	no space charge low or high field transport (standard charge transport)
2	$t^M > t_t$	space charge exists nonsteady state T-SCLC
3	$t^M = t_t$	space charge exists steady state S-SCLC (present paper)

Let us suppose for the purpose of the present paper that we apply a constant external voltage on the sample. If the Maxwell relaxation time is less than the corresponding transit time (Case 1), the injected carriers do not manage to cross the sample as the movement of the equilibrium carriers neutralizes their charge. So, in this case, the "classical" low- or high-field transport is observed. The crucial case for the purpose of the present paper is Case 3, where the equilibrium between the transit and the Maxwell relaxation times occurs. The injected carriers experience the full transit, so that after their extraction an exactly equal number of carriers is injected from the injection contact. This situation bears all the features of the *self-controlled steady-state process* and may be kept for infinite time. If *e.g.* a small perturbation increases the voltage on the sample, thus decreasing the transit time, the conductivity of the sample has to rise correspondingly (shifting the quasi-Fermi level) in order to reintroduce a new steady-state situation (the higher value of the current).

Combining eqns (*1*) and (*2*) in the preceeding paper in this issue we obtain the condition for the onset of the S-SCLC

$$U_{crit} = \frac{e n_f L^2}{\varepsilon \varepsilon_0 \Theta(U_{crit})} \qquad (1)$$

and the corresponding current density

$$i_{SCLC}(U) = \frac{cU}{t_t} = \frac{\varepsilon \varepsilon_0 \mu_0 \Theta(U) U^2}{L^3} \qquad (2)$$

where c is the geometrical capacitance of the sample and the distribution function $\Theta(U) = n_f/(n_f + n_s)$, where n_f and n_s are the concentrations of free and trapped charge carriers (electrons), respectively. Eqn (*2*) is the simplified version of the SCLC master equation. At this moment it should be pointed out that the spectroscopical character of the SCLC is to be found in the distribution function $\Theta(U)$, containing information on the space charges in traps, and also on the steady-state drift mobility $\mu_d = \mu_0 \cdot \Theta$.

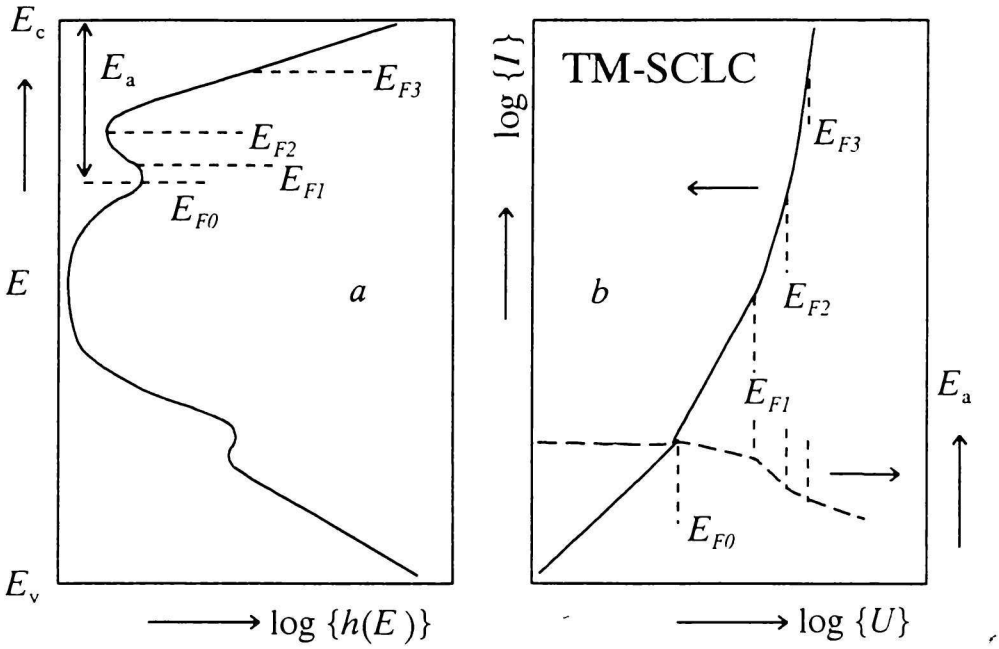

Fig. 1. *a*) The artificial DOS with the steady-state Fermi level position E_{F0}, and several quasi-Fermi levels E_{Fi}. *b*) The corresponding $I(U)$ dependence (and also corresponding activation energy—voltage $E_a(U)$ dependence) pertinent to the TM-SCLC method [8, 9].

In order to illuminate the S-SCLC method, we depicted schematically in Fig. 1*a* the artificial DOS function $h(E)$ with the steady-state Fermi level position E_{F0}, and in Fig. 1*b* the corresponding current voltage $I(U)$ dependence (and also corresponding activation energy—voltage $E_a(U)$ dependence pertinent to the TM-SCLC method [8, 9]). The gist of the method is very simple: by increasing the voltage on the sample, the quasi-Fermi level is shifted upwards, so filling the trapping states (*e.g.* in the interval $E_{F0} - E_{F1}$ of the Fermi level shift). These states are reflected in the resulting $I(U)$ characteristics in a straightforward manner – the higher is the DOS, the lower is the slope $m = \mathrm{d}(\ln I)/\mathrm{d}(\ln U)$, the limiting lowest value being $m = 2$. So, it is only necessary to find a proper mathematical framework for DOS reconstruction. It is worth mentioning that the measured activation energy E_a serves for the independent energy reconstruction of the measured DOS [8, 9].

Steady-State Space-Charge-Limited Currents

In the following we will adopt the same procedure and assumptions as used in [8]. We start from conventional equations, the Ohm's law in the form [8—10]

$$j = e\mu_0\, n_f(x)\, F(x) + eD\,\frac{\mathrm{d}n_f(x)}{\mathrm{d}x} \qquad (3)$$

and from the Poisson equation

$$\frac{\mathrm{d}F(x)}{\mathrm{d}x} = -\frac{e[n_s(x) - \overline{n}_s]}{\varepsilon\varepsilon_0} \qquad (4)$$

where j is the current density, μ_0 is the microscopic mobility, supposed to be constant, $F(x)$ the electric field strength, $n_f(x)$ the concentration of free carriers (electrons), $n_s(x)$ the total concentration of carriers (electrons, both free and trapped). The term $e[n_s(x) - \overline{n}_s]$ then represents the space-charge density in the sample, $\overline{n}_s$ is the total concentration of carriers in the thermodynamic equilibrium. Further, with the exception of the last chapter (S-SCLC in real situations) we neglect for tractability of expressions the second term in eqn (*3*) representing the diffusion current.

The combination of the first derivative of eqn (*3*) with respect to coordinate and the Poisson equation (*4*) gives

$$\frac{\mathrm{d}n_f}{\mathrm{d}x} = \frac{e\mu_0}{j}\,\frac{e}{\varepsilon\varepsilon_0}\, n_f^2\,(n_s - \overline{n}_s) \qquad (5)$$

and integrating along the sample, we have

$$\frac{1}{j} = \frac{1}{e\mu_0 L}\,\frac{\varepsilon\varepsilon_0}{e}\int_{n_{fc}}^{n_{fL}} \frac{\mathrm{d}n_f}{n_f^2(n_s - \overline{n}_s)} \equiv Y \qquad (6)$$

where we use the position index L defined $n_{fL} = n_f(x = L)$ and the value n_{fc} is for the free carrier concentration at the cathode ($n_{fc} \to \infty$).

Using now the obvious expression for the electric field strength combined with the expression (*3*), we

obtain

$$-\mathrm{d}U = F\mathrm{d}x = \left(\frac{j}{e\mu_0 n_\mathrm{f}}\right)\mathrm{d}x = \\ = \left(\frac{j}{e\mu_0}\right)^2 \frac{\varepsilon\varepsilon_0}{e}\frac{\mathrm{d}n_\mathrm{f}}{n_\mathrm{f}^3(n_\mathrm{s}-\overline{n}_\mathrm{s})} \qquad (7)$$

Integrating again along the sample then gives finally

$$\frac{U}{j^2} = \frac{\varepsilon\varepsilon_0}{e(e\mu_0)^2}\int_{n_{\mathrm{fc}}}^{n_{\mathrm{fL}}}\frac{\mathrm{d}n_\mathrm{f}}{n_\mathrm{f}^3(n_\mathrm{s}-\overline{n}_\mathrm{s})} \equiv Z \qquad (8)$$

Eqns (*6*) and (*8*) are crucial for SCLC theory, as they bring the SCLC $j(U)$ characteristic in the parametric form in terms of the DOS contained in terms of space charge.

For the purpose of modelling we compiled the modelling program SNOVAL [11]. The model calculations are straightforward. Input information for the program SNOVAL are the parameters of the DOS function $h(E)$, temperature T, and the other parameters mentioned above. Then, choosing independently the position of the quasi-Fermi level, we first calculate the current density using eqn (*6*) and then voltage across the sample using eqn (*8*). The space-charge density is expressed in terms of total and free concentrations of carriers, n_s and n_f, respectively. The most difficult step is to calculate the activation energy E_a using the definition as we must take into account the temperature statistical shift of the quasi-Fermi level. This is achieved by a time-consuming iteration procedure using eqns (*6*) and (*8*) for slightly increased temperature $T + \mathrm{d}T$, as long as we do not obtain the same voltage U across the sample as at the temperature T. Then the corresponding changes of the current j make it possible to calculate the activation energy E_a.

The mathematical apparatus for DOS reconstruction from TM-SCLC data is explained elsewhere [8, 9], here it is worth mentioning that using the equation for the current and the Poisson equation with proper boundary conditions, we obtain for the value of the DOS function

$$h(E) \approx \frac{\mathrm{d}n_{\mathrm{s}L}}{\mathrm{d}E_F} = \frac{1}{kT}\frac{\varepsilon\varepsilon_0 U}{eL^2}\frac{2m-1}{m^2}(1+C) \qquad (9)$$

where $\varepsilon\varepsilon_0$ is the permittivity, $m = \mathrm{d}(\ln I)/\mathrm{d}(\ln U)$ is the first derivative of the $\log(I)$ *vs.* $\log(U)$ dependence, and C is a second-order term including higher derivatives of the $I(U)$ characteristic

$$C = \frac{B(2m-1) + B^2(3m-2) + \mathrm{d}[\ln(1+B)]/\mathrm{d}(\ln U)}{1+B(m-1)} \qquad (10)$$

where $B = -[\mathrm{d}m/\mathrm{d}(\ln U)]/[m(m-1)(2m-1)]$. As the right-hand side of eqn (*9*) is accessible from experiment, this equation gives, after the deconvolution with respect to the known statistical functions, the unknown $h(E)$ DOS distribution.

The corresponding energy is then

$$E = E_\mathrm{a} + \frac{\mathrm{d}(\ln\mu_0)}{\mathrm{d}(1/kT)}\frac{2m-3}{m(2m-1)}\frac{\mathrm{d}E_\mathrm{a}}{\mathrm{d}(\ln U)} + \\ + \frac{1}{1+C}\frac{\mathrm{d}C}{\mathrm{d}(1/kT)} \qquad (11)$$

where E_a is the measured activation energy of S-SCLC ($E_\mathrm{a} = -\mathrm{d}(\log I)/\mathrm{d}(1/kT)$).

The steady-state drift mobility is also accessible from the measured data

$$\mu_\mathrm{eff} = \mu_0\Theta = \\ = \frac{jL^3}{\varepsilon\varepsilon_0 U^2}\left[\left(\frac{m-1}{m}\right)\left(\frac{2m-1}{m}\right)^2(1+B)\right]^{-1} \qquad (12)$$

where again B is the correction term with higher derivatives.

For the reconstruction of so obtained data of $j(U)$ and $E_\mathrm{a}(U)$ characteristics we applied the reconstruction program RECON [12] that principally uses eqns (*9—11*) and a spline deconvolution procedure.

APPLICATION OF THE METHOD

In Figs. 2—4 there are calculated, near to reality model examples of S-SCLC. The purpose of the figures is to give an idea of the potential information obtained.

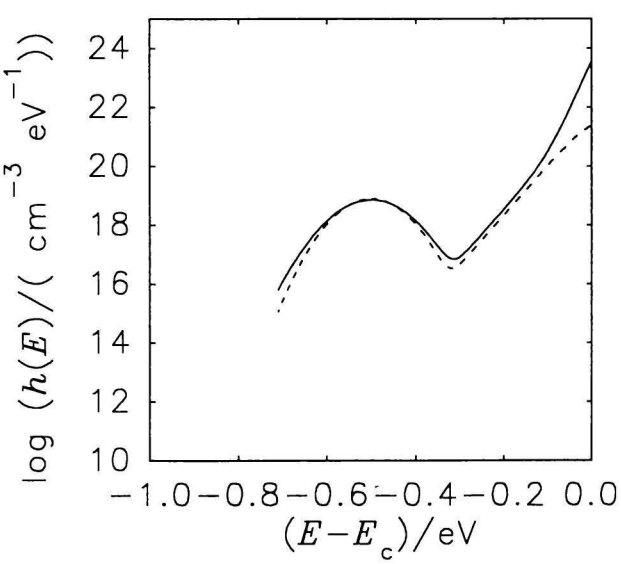

Fig. 2. The illustrative input DOS formed by the Gaussian distribution (σ = 0.05 eV, E_t = 0.5 eV, $N_\mathrm{t} = 1 \times 10^{18}$ cm^{-3}) and tail states (kT_c = 30 meV) (continuous line), the reconstruction of the DOS using the program RECON [12] is also depicted (by a dashed line).

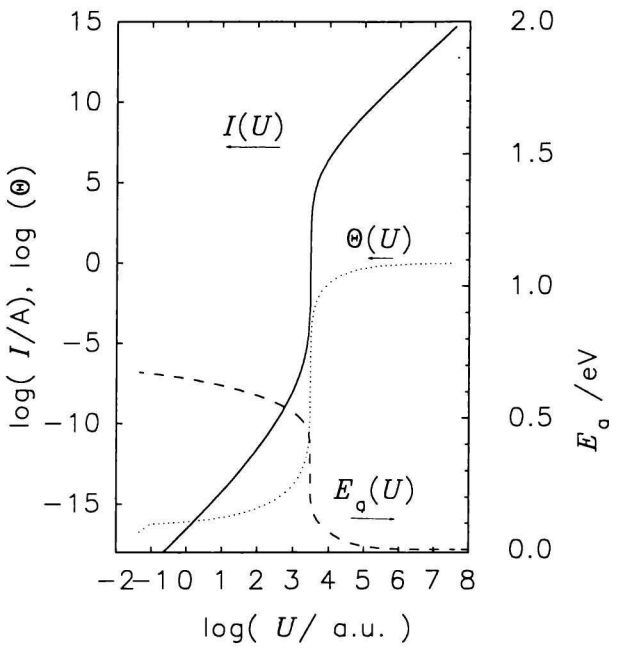

Fig. 3. The $I(U)$ (continuous line) and $E_a(U)$ (dashed line) characteristics calculated by the Stöckmann iterative procedure [10] (using the program SNOVAL [11]), also the distribution function $\Theta(U)$ is depicted (dotted line), $T = 150$ K.

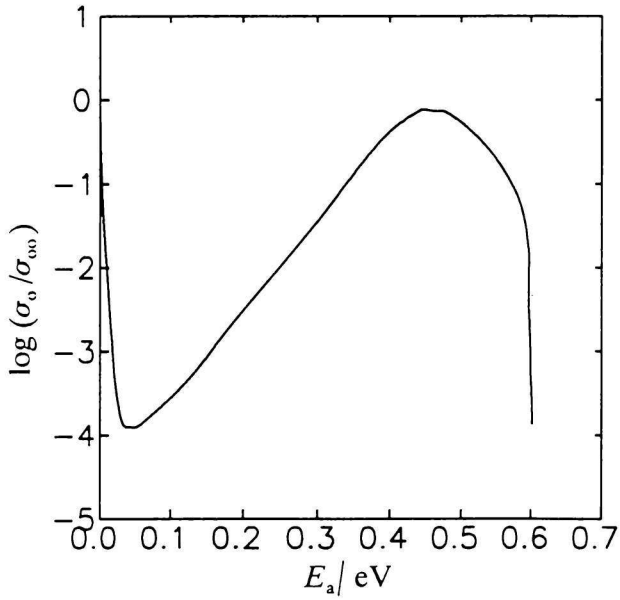

Fig. 4. The dependence of the fictive conductivity preexponential factor σ_0 on the activation energy E_a for S-SCLC given in Fig. 3, but for $T = 300$ K.

Possibilities and Limitations of the S-SCLC Method

To show the applicability of the TM-SCLC method to study various DOS distributions in more detail, we calculated model characteristics with respect to such experimental variables as are temperature and the parameters of the DOS distribution, and as are the widths of the distribution, the total concentration of states and their energy position.

For the modelling we used the following parameters for the DOS double exponential distribution: $T_t = 300$ K and $N_t = 1 \times 10^{14}$ cm^{-3}, situated in the interval $E_t \in (-0.8, -0.2)$ eV, for the transport band we used $h(E_c) = 4 \times 10^{22}$ cm^{-3} eV^{-1}, $E_c = 0$ eV, all for $T = 150$ K.

In Fig. 5 there are collected the model space charge-forming characteristics, *i.e.* the increment of the space charge dn_s/dE_{Fn} (*a*), the activation energy E_a (*b*), and the statistical shift of the quasi-Fermi level $kT\gamma_F$, all at the position of the quasi-Fermi level, in Fig. 6 the corresponding TM-SCLC characteristics, *i.e.* current—voltage $j(U)$ and activation energy—voltage $E_a(U)$ dependences and in Fig. 7 the reconstructed DOS function $h(E)$ compared with the input DOS function, all these with the position of the maximum of the double-exponential DOS distribution E_t as a parameter.

As we have chosen the condition $T < T_t$, we will be able to "see" and reconstruct the DOS for the peak position of the DOS distribution $E_c - E_t < 0.4$ eV, which is obvious from Figs. 5*a* and 5*b*, from the SCLC characteristics in Fig. 6 and especially from the reconstruction in Fig. 7. The SCLC data for $E_c - E_t > 0.4$ eV do not bring the deserved information about the double exponential DOS, as the contribution to the space charge from the free carriers in the transport band strongly predominates.

Resolving Power of the S-SCLC Method

In order to examine the theoretical limits of the TM-SCLC method for DOS recovering procedures in exponentially **decreasing part** of the distribution of DOS function we used two superimposed bell-shape DOS functions, the first with $T_t = 200$ K, $N_t = 10^{18}$ cm^{-3}, and $E_t = -0.9$ eV defined by

$$h(E) = \frac{N_t}{kT_t} \frac{\exp\left(\frac{E - E_t}{kT_t}\right)}{\left[1 + \exp\left(\frac{E - E_t}{kT_t}\right)\right]^2} \qquad (13)$$

and the second with $T_x = 100$ K, as a superimposed perturbation of the constant value above the first bell-shape distribution

$$h(E) = \frac{N_x}{kT_x} \frac{\exp\left(\frac{E - E_x}{kT_x}\right)}{\left[1 + \exp\left(\frac{E - E_x}{kT_x}\right)\right]^2} \qquad (14)$$

with changing position of E_x, further we used $L = 100$ μm and $\varepsilon_r = 3$.

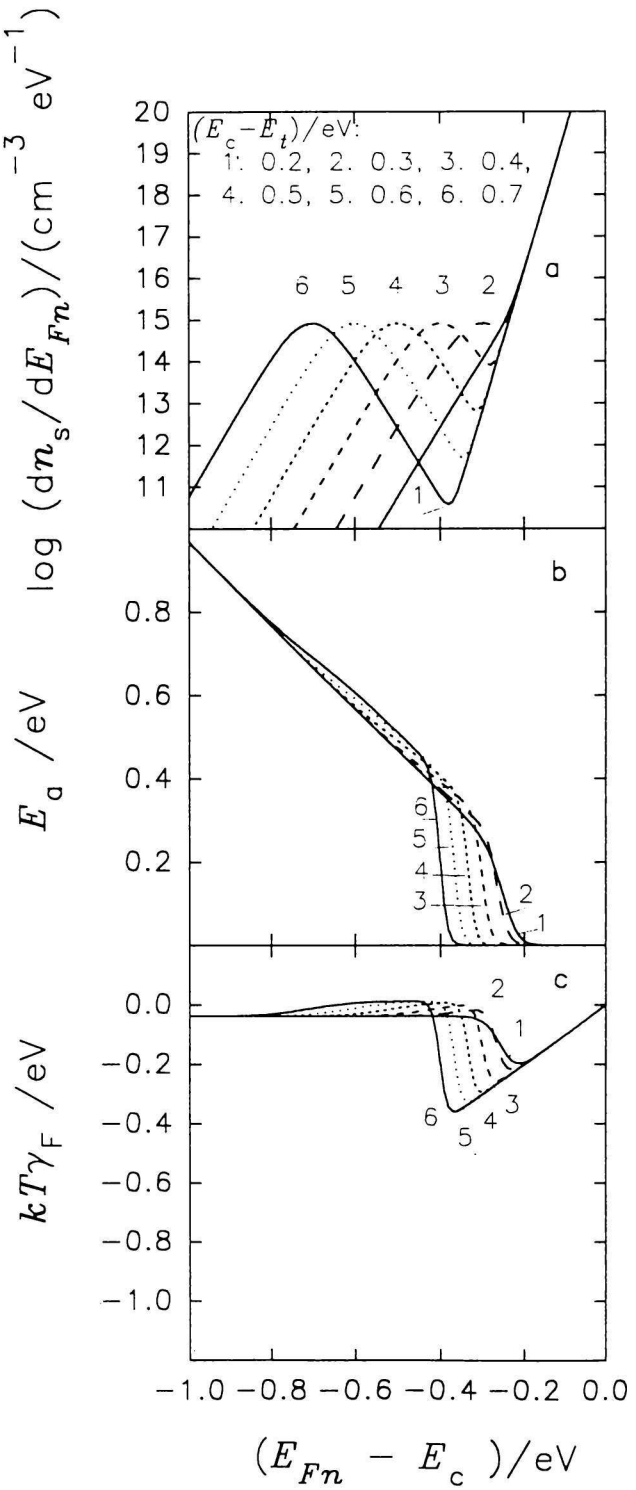

Fig. 5. The influence of the energy position of the distribution $(E_c - E_t) \in$ (0.2 eV, 0.8 eV): the SCLC model for states with double exponential distribution in energy with $N_t = 1 \times 10^{14}$ cm^{-3}, $T_t = 300$ K, and $T = 100$ K. *a*) The increment of the space charge $\mathrm{d}n_s/\mathrm{d}E_{Fn}$; *b*) the activation energy E_a; *c*) the statistical shift of the quasi-Fermi level $kT\gamma_F$, at the quasi-Fermi level E_{Fn}.

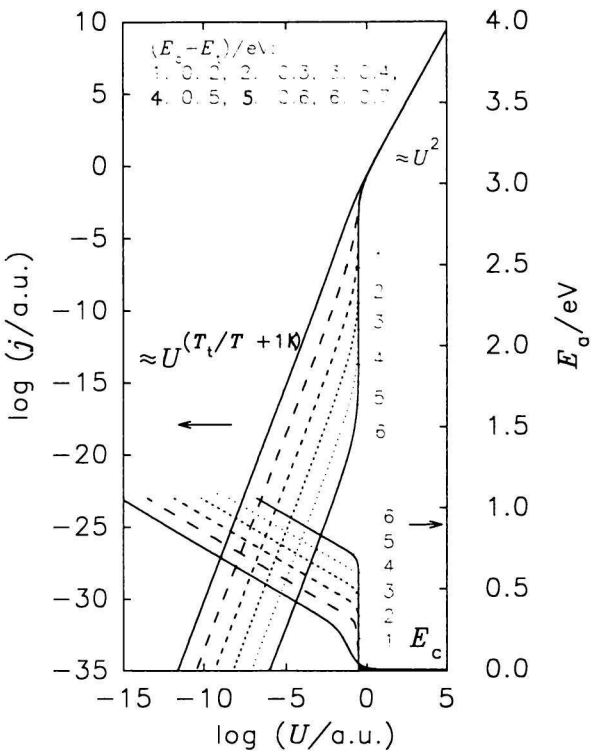

Fig. 6. The TM-SCLC model for the situation from Fig. 5: the current—voltage characteristics $j(U)$ and the activation energy—voltage characteristics $E_a(U)$.

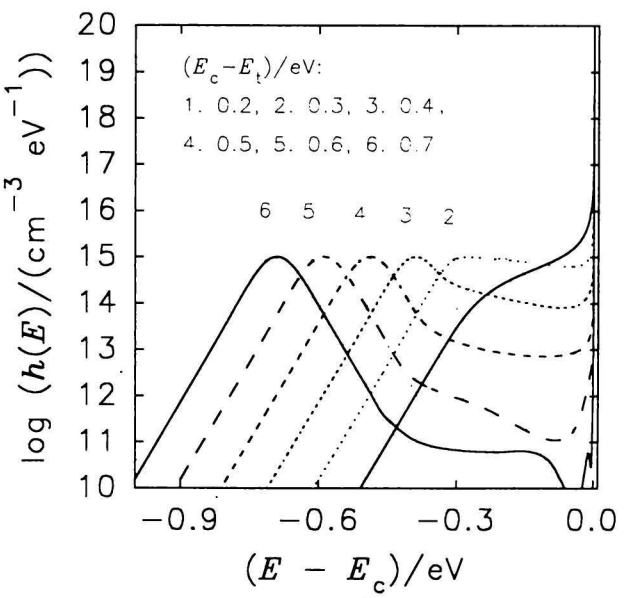

Fig. 7. The DOS functions $h(E)$ obtained using the program RECON and the procedure described in the text from the data in Fig. 6 compared with the input DOS functions.

In Fig. 8 is the first model. In Fig. 8*a* is the input DOS function $h(E)$. In Fig. 8*b* is the output of the numerical evaluation of the data in Fig. 8*a*, giving the logarithm of the reverse slope $\log(1/m)$, $m = \mathrm{d}(\ln j)/\mathrm{d}(\ln U)$ and the term $\log|C|$ with higher

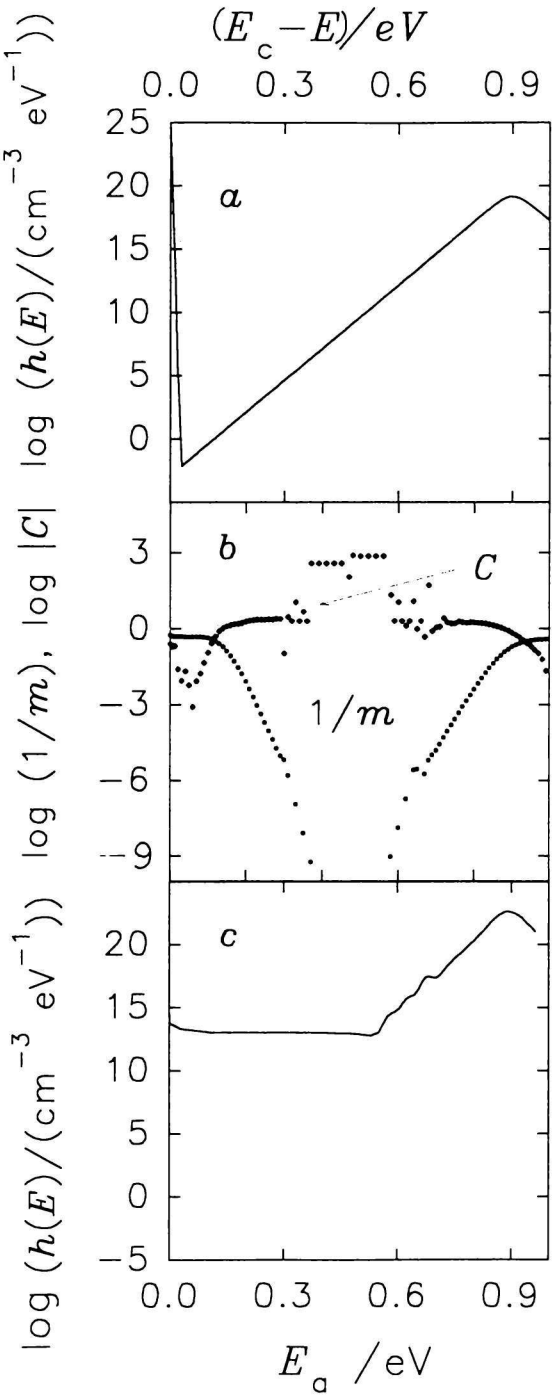

Fig. 8. The input and reconstruction of the TM-SCLC data for the double exponential distribution of states. *a*) The input DOS function; *b*) the slope $1/m$ and the term C (eqn (*10*)); *c*) the reconstruction of the DOS function using the program RECON.

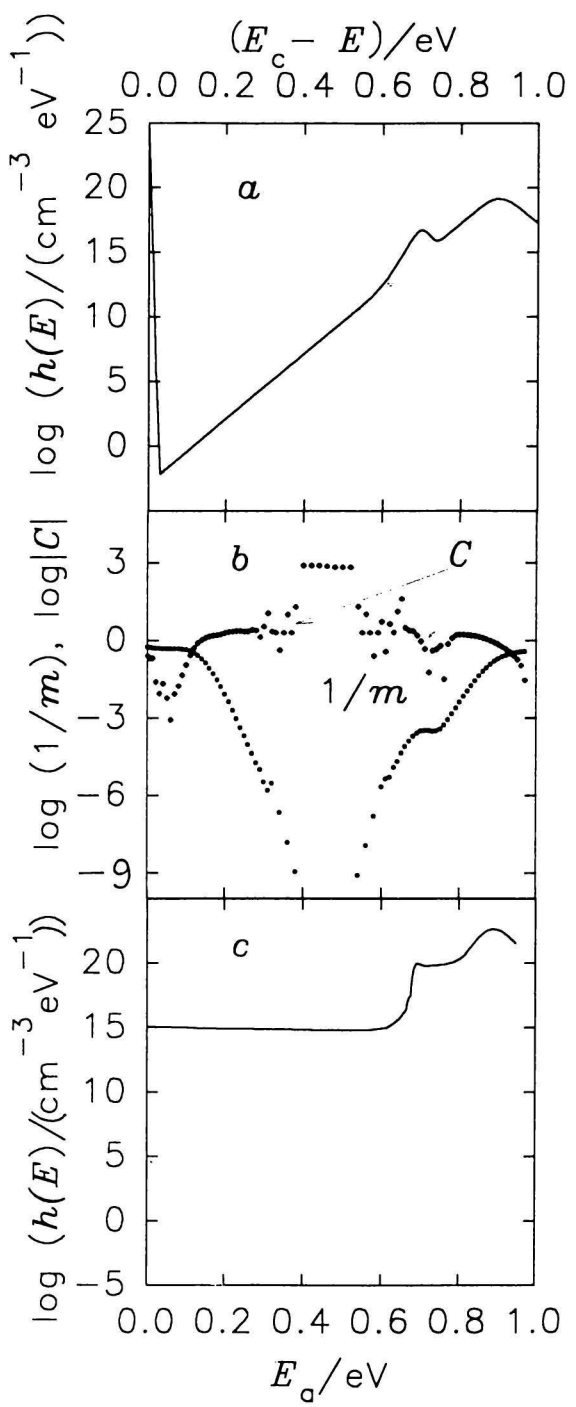

Fig. 9. The input and reconstruction of the TM-SCLC data with the position of the "bump" at $E_x = -0.7$ eV. *a*) The input DOS function; *b*) the slope $1/m$ and the term C (eqn (*10*)); *c*) the reconstruction of DOS function using the program RECON.

derivatives from eqn (*10*) on energy. Then, in Fig. 8*c* is the result of DOS function reconstruction using eqns (*9*) and (*11*). It is obvious that the **exponentially decreasing part of the distribution** was properly reconstructed up to $E = -0.55$ eV, *i.e.* about 10 orders of magnitude below the maximum of the distribution. Obviously, the limiting step in the reconstruction is the resolution of the mathematics used, as we found by this numerical experiment that the limiting stable point is given by the limiting slope corresponding to $m \approx 10^5$!! This is obviously not accessible in a real experiment, but is rather a measure of the precision of

the modelling and evaluation processes and the consistency of the S-SCLC method (and especially of its TM-SCLC modification).

To learn something more about the resolving power of the reconstruction in the region of decreasing part of the DOS distribution, we used the data depicted in part *a* of Fig. 9, where we superimposed a small perturbation in an exponentially decreasing DOS in a form of a small "bump" at the energy position $E_x = -0.7$ eV. The reconstruction depicted in Fig. 9*c* gives reasonable reconstruction.

Amphoteric Defects

Let us consider further electron injection into a model semiconductor of the bandgap ΔE_g with localized amphoteric defect states situated at the energy E_t with respect to the conduction transport band located at energy $E_c = 0$, the effective concentration of transport states is assumed to be N_c. The defects are characterized by an effective correlation energy U, which may be either positive, $U > 0$, or negative, $U < 0$, depending on the lattice distortions, caused by the occupation of the defect [13]. The injection of holes may be treated in a straightforward way. The statistics of amphoteric states differs from the Fermi—Dirac statistics and the probabilities [14—16] for the defect being unoccupied, F^+, singly occupied, F^0, and doubly occupied, F^-, are the function of the quasi-Fermi level E_{Fn}

$$F^+ = \frac{1}{1 + 2e^{\frac{(E_{Fn}-E_t)}{kT}} + e^{\frac{(2E_{Fn}-2E_t-U)}{kT}}} \qquad (15)$$

$$F^0 = 2e^{\frac{(E_{Fn}-E_t)}{kT}} F^+ \qquad (16)$$

$$F^- = e^{\frac{(2E_{Fn}-2E_t-U)}{kT}} F^+ \qquad (17)$$

where k is the Boltzmann constant and T is the temperature.

Let us further suppose the existence of monoenergetic amphoteric states of the concentration N_t with the correlation energy U, situated at the energy E_t with respect to the conduction transport band located at energy E_c. For the description of the space charge formation the knowledge of the electron concentration in amphoteric states of all three charge states is decisive. We can write for the concentration of doubly occupied, n^-, singly occupied, n^0, and unoccupied, n^+, states the following equations

$$n^- = N_t F^- \qquad (18)$$

$$n^0 = N_t F^0 \qquad (19)$$

$$n^+ = N_t F^+ \qquad (20)$$

where the obvious condition $n^- + n^0 + n^+ = N_t$ must be valid. The corresponding increments of the respective concentrations due to the shift of the quasi-Fermi level then are

$$\frac{dn^+}{d\left(\frac{E_{Fn}}{kT}\right)} = 2N_t \frac{dF^+}{d\left(\frac{E_{Fn}}{kT}\right)} =$$

$$= \frac{2N_t \left[e^{\frac{(E_{Fn}-E_t)}{kT}} + e^{\frac{(2E_{Fn}-2E_t-U)}{kT}}\right]}{\left[1 + 2e^{\frac{(E_{Fn}-E_t)}{kT}} + e^{\frac{(2E_{Fn}-2E_t-U)}{kT}}\right]^2} \qquad (21)$$

$$\frac{dn^0}{d\left(\frac{E_{Fn}}{kT}\right)} = 2N_t \frac{dF^0}{d\left(\frac{E_{Fn}}{kT}\right)} =$$

$$= \frac{2N_t \left[e^{\frac{(E_{Fn}-E_t)}{kT}}\right]\left[1 - e^{\frac{(2E_{Fn}-2E_t-U)}{kT}}\right]}{\left[1 + 2e^{\frac{(E_{Fn}-E_t)}{kT}} + e^{\frac{(2E_{Fn}-2E_t-U)}{kT}}\right]^2} \qquad (22)$$

$$\frac{dn^-}{d\left(\frac{E_{Fn}}{kT}\right)} = 2N_t \frac{dF^-}{d\left(\frac{E_{Fn}}{kT}\right)} =$$

$$= \frac{2N_t \left[e^{\frac{(2E_{Fn}-2E_t-U)}{kT}}\right]\left[1 - e^{\frac{(E_{Fn}-E_t)}{kT}}\right]}{\left[1 + 2e^{\frac{(E_{Fn}-E_t)}{kT}} + e^{\frac{(2E_{Fn}-2E_t-U)}{kT}}\right]^2} \qquad (23)$$

where

$$\frac{dn^+}{d\left(\frac{E_{Fn}}{kT}\right)} + \frac{dn^-}{d\left(\frac{E_{Fn}}{kT}\right)} + \frac{dn^0}{d\left(\frac{E_{Fn}}{kT}\right)} = 0$$

The net space charge in the sample is then the difference between the total concentration of electrons, n_s, and their thermodynamical concentration, $\overline{n}_s$. For the total concentration of electrons it may be written

$$n_s = n^0 + 2n^- + n_f \qquad (24)$$

and for its increment due to the shift of the quasi-Fermi level

$$\frac{dn_s}{d\left(\frac{E_{Fn}}{kT}\right)} = \frac{dn^0}{d\left(\frac{E_{Fn}}{kT}\right)} + 2\frac{dn^-}{d\left(\frac{E_{Fn}}{kT}\right)} + \frac{dn_f}{d\left(\frac{E_{Fn}}{kT}\right)} \qquad (25)$$

where n_f is the concentration of free (delocalized) electrons which can be approximated by the relation $n_f = N_c \exp(E_{Fn} - E_c)/kT$. The coefficient 2 in eqns (*24*) and (*25*) expresses the occupancy of the state by two electrons. For the sake of simplicity we will further neglect the thermodynamical concentration $\overline{n}_s$ with respect to the total concentration n_s. In fact, this means that n_s is directly the concentration of electrons forming the injected space charge in the sample and

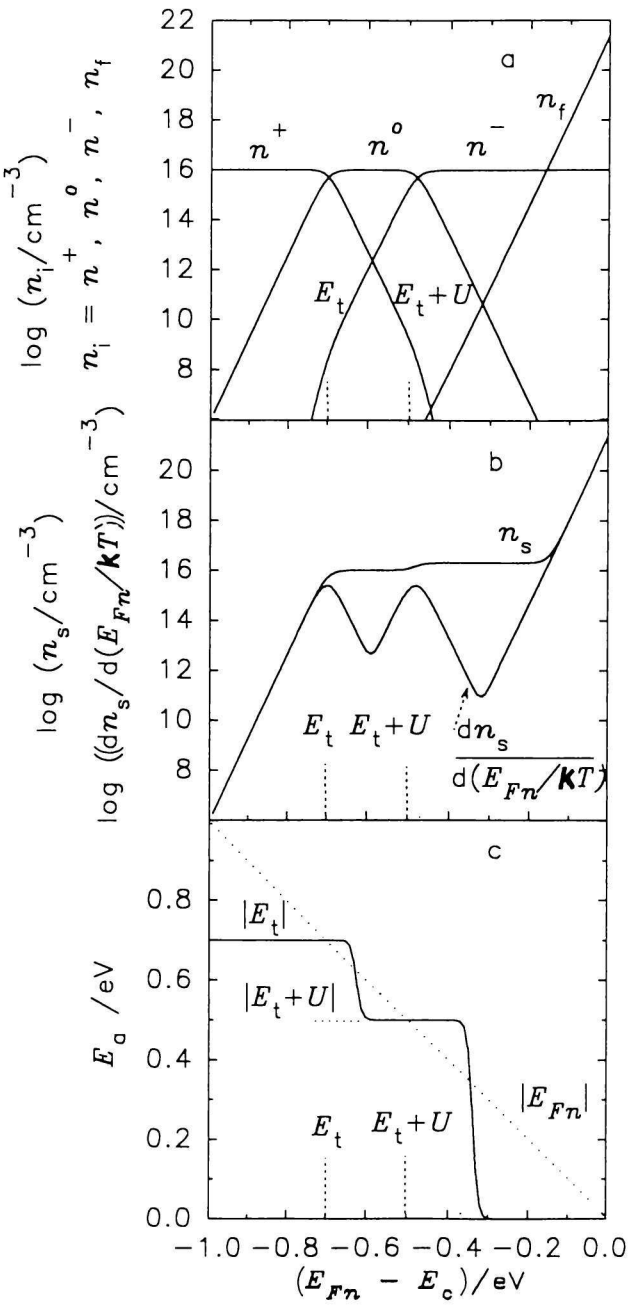

Fig. 10. The SCLC model for monoenergetic amphoteric states with **positive** correlation energy U located at the energy E_t. *a*) The contributions to the space charge of different charge states concentrations n^+, n^0, and n^-, and concentration of free charge carriers n_f; *b*) total concentration of electrons n_s forming the space charge and its increment $dn_s/d(E_{Fn}/kT)$; *c*) activation energy E_a, the dotted line gives the position of the quasi-Fermi level, all characteristics are plotted at the position of the quasi-Fermi level E_{Fn}.

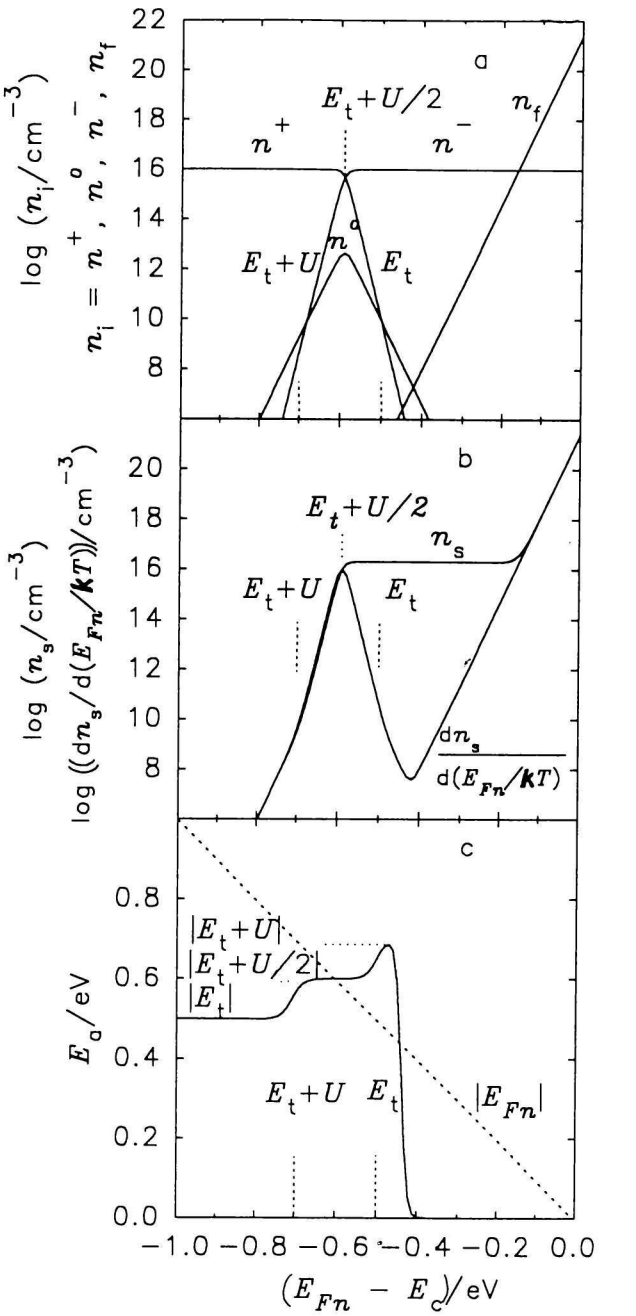

Fig. 11. The SCLC model for monoenergetic amphoteric states with **negative** correlation energy U located at the energy E_t. *a*) The contributions to the space charge of different charge states concentrations n^+, n^0, and n^-, and concentration of free charge carriers n_f; *b*) total concentration of electrons n_s forming the space charge and its increment $dn_s/d(E_{Fn}/kT)$; *c*) activation energy E_a, the dotted line gives the position of the quasi-Fermi level, all characteristics are plotted at the position of the quasi-Fermi level E_{Fn}.

$dn_s/d(E_{Fn}/kT)$ its increment due to the shift of the quasi-Fermi level.

In Figs. 10 and 11, the space charge-forming characteristics are given of the amphoteric states for positive ($U > 0$, Fig. 10) and negative ($U < 0$, Fig. 11) correlation energy. In part *a* of both figures, the contributions to the space charge of different charge states having concentrations n^+, n^0, and n^- (according to

eqns (*18—20*)), and concentration of free charge carriers n_f are given. In part *b* the corresponding total concentration of electrons n_s forming the space charge and its increment $dn_s/d(E_{Fn}/kT)$ are given, all at the position of the quasi-Fermi level (according to eqns (*18—25*). In part *c* of both figures the activation energy E_a is plotted at the position of the quasi-Fermi level.

The inspection of the occupation statistics of the amphoteric states with positive correlation energy in Fig. 10 reveals that the states behave like two separate singly occupied states of the same concentration N_t, situated at the energies E_t and $E_t + U$ (see the increment $dn_s/d(E_{Fn}/kT)$ in Fig. 10*b*). Physically this means that by shifting of the quasi-Fermi level (*e.g.* by injection) from the side of lower energies ($E_{Fn} < E_t$) the predominant transition $D^+ + e \rightarrow D^0$ takes place first, whereas the second transition $D^0 + e \rightarrow D^-$ takes over when the quasi-Fermi level is situated above the energy $E_t + U/2$ and the second fictive state situated at $E_t + U$ is occupied. In other words, due to the positive value of the correlation energy ($U > 0$), the occupation of the amphoteric states by two electrons is accomplished in two separate and successive steps. This fact is supported by the dependence of the dominant energy E_a on the quasi-Fermi level position (see plateaus in Fig. 10*c* situated at the energies $|E_t|$ and $|E_t + U|$).

An entirely different behaviour is apparent from Fig. 11 for the amphoteric states with $U < 0$. To the first approximation, they behave like doubly occupied states of the concentration N_t, situated at the energy $E_t + U/2$. The physical reason for this behaviour is that it is energetically more favourable to occupy the amphoteric state D^+ by two electrons in a single step, $D^+ + 2e \rightarrow D^-$; for this process the total energy supplied is $2\Delta E_g + 2E_t + U$ (and the average energy per one electron required for this occupation is $\Delta E_g + E_t + U/2$), then to supply two successive electrons forming D^0 states, $D^+ + e \rightarrow D^0$, with the energy cost $\Delta E_g + E_t$, and finally to form D^- states, $D^0 + e \rightarrow D^-$ with the energy cost $\Delta E_g + E_t + U$. However, the overview of Fig. 11*c* in detail gives more information. On shifting the quasi-Fermi level from the side of lower energies ($E_{Fn} < E_t + U$) the transition $D^+ + e \rightarrow D^0$ occurs first (the corresponding dominant energy E_a for this transition being $|E_t|$) as the transition forming D^- states is highly improbable in this energy region. Then, in the energy interval of the quasi-Fermi level $E_{Fn} \in (E_t + U, E_t)$ the transition $D^+ + 2e \rightarrow D^-$ prevails, resulting in the increase of the activation energy to the value $E_a = |E_t + U/2|$. When the quasi-Fermi level is located above $E_{Fn} > E_t$, then $E_a = |E_t + U|$ since prevailing transitions are $D^0 + e \rightarrow D^-$; as there are nearly no D^+ states available in the sample at these positions of the quasi-Fermi level.

In Figs. 12 and 13 are the calculated SCLC characteristics for monoenergetic amphoteric states with both the positive ($U > 0$, Fig. 12) and negative ($U < 0$, Fig. 13) correlation energies. As we have discussed in connection with the space charge-forming characteristics, the $j(V)$ and $E_a(V)$ (where now V is the applied voltage on the sample) dependences for $U > 0$ behave like two monoenergetic states, situated at E_t and $E_t + U$. Consequently, the $j(V)$ characteristic starts for a low voltage (*i.e.* for the position of the quasi-Fermi level $E_{Fn} < E_t$) with the slope $m = d(\ln j)/d(\ln U) = 2$, typical of a monoenergetic state. Corresponding transitions are $D^+ + e \rightarrow D^0$, *i.e.* electrons injected into the sample occupy the D^+ states, transforming them to the D^0 states. Then, the corresponding measured activation energy is $E_a = |E_t|$. On increasing the voltage and shifting the quasi-Fermi level by charge injection, the transition to the second charge state situated at the energy $E_t + U$ occurs, *i.e.* $D^0 + e \rightarrow D^-$. The corresponding activation energy is then changed accordingly, *i.e.* $E_a = |E_t + U|$. For higher voltages, the trap-filled limit region occurs, manifested by the increase of the current by many orders of magnitude and by corresponding decrease in the activation energy to the zero value, followed by the Child law [1], $j \approx V^2$.

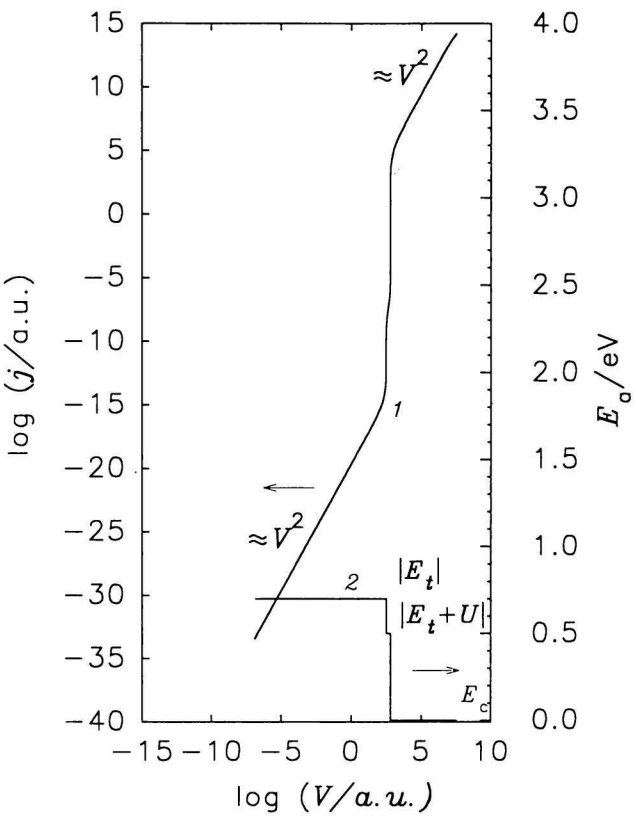

Fig. 12. The temperature modulated SCL current model for the situation from Fig. 10. *1.* The current—voltage characteristics $j(V)$; *2.* the activation energy—voltage characteristics $E_a(V)$.

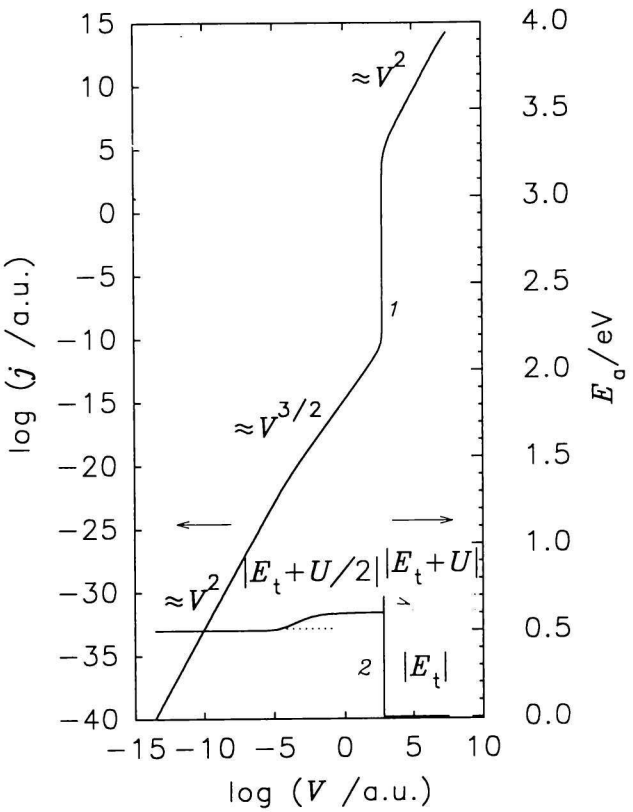

Fig. 13. The temperature modulated SCL current model for the situation from Fig. 11. *1.* The current—voltage characteristics $j(V)$; *2.* the activation energy—voltage characteristics $E_a(V)$.

The SCLC characteristic for the case of states with $U < 0$ (Fig. 13) looks entirely different. For low applied voltages, when the quasi-Fermi level is positioned at $E_{Fn} < E_t + U$, the predominant one-electron transition $D^+ + e \rightarrow D^0$ takes place, so that the slope of the $j(V)$ characteristic is, as expected, $m = 2$ and the corresponding activation energy is $E_a = |E_t|$. On shifting the quasi-Fermi level above $E_t + U$, the two-electron transition $D^+ + 2e \rightarrow D^-$ occurs, resulting in the decrease of the slope of the $j(V)$ characteristic to $m = 1.5$ and in the increase of the activation energy to $E_a = |E_t + U/2|$. This behaviour is unique in the SCLC theory, as the minimal slope of $j(V)$ characteristic in SCLC regime was considered to be $m_{crit} = 2$. This peculiarity for the amphoteric states with $U < 0$ is associated with the decrease of the value of the distribution coefficient with the shift of the quasi-Fermi level in the energy interval $E_{Fn} \in (E_t + U, E_t)$ and the resulting $j(V)$ characteristics

$$\theta = \frac{n_f}{n_s} = \frac{n_f}{n^0 + 2n^- + n_f} = \frac{N_c}{N_t} e^{\frac{-E_F - E_c + U + 2E_0}{kT}} \quad (26)$$

$$j = \left[\left(\frac{4}{3}\right)^3 \frac{\varepsilon_0 \varepsilon e N_c^2 \mu^2}{L^4 N_t} e^{\frac{2E_0 + U - 2E_c}{kT}} \right]^{\frac{1}{2}} V^{\frac{3}{2}} \quad (27)$$

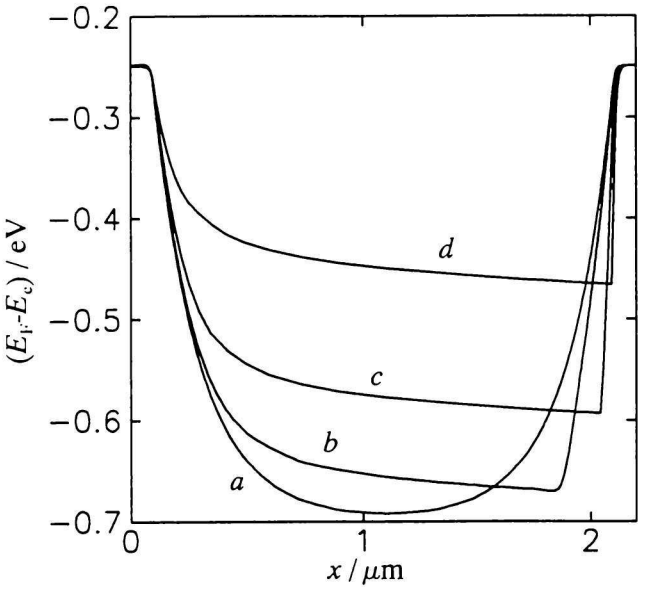

Fig. 14. Spatial energy band profiles $E_F - E_c$ in the n–i–n device under S-SCLC at zero bias (*a*) and at different applied voltages: $U = 1.1$ V (*b*), 4.8 V (*c*), 11.1 V (*d*).

Also the increase in the activation energy E_a with the shift of the quasi-Fermi level towards the transport band was not envisaged with the localized states without correlation effects and it is associated with the predominant occupation step of D^+ states simultaneously by two electrons as described in this paper. Further shift of the quasi-Fermi level towards the transport band makes it possible to convert the D^0 states to D^- states ($D^0 + e \rightarrow D^-$) with the corresponding $j \approx V^2$ dependence and the increase of the activation energy to the value of $E_a = |E_t + U|$.

S-SCLC in Real Situations

In the last part of this paper we present the results of exact model calculations, closely related to the situations encountered in real samples. Especially we tested the existence of non-infinite charge-carrier reservoirs at the contacts and the neglectance of the diffusion currents in eqn (*3*). For this purpose we numerically modeled S-SCLC for a "real device" formed by n–i–n structure of amorphous hydrogenated silicon (where n marks strongly N doped regions and i marks intrinsic material). For the numerical calculations we used eqns (*3*) and (*4*). The details of the modelling calculations are given elsewhere [17], here we extract the main results.

In Fig. 14 is the energy spatial profile of the conduction band diagram of the model n–i–n structure, parametric in the applied voltage, *i.e.* differing in the value of the space-charge-limited current. It is necessary to note that the injecting contact is the left one, the right one serves for the extracting purposes only and does not influence SCLC markedly. Interesting is

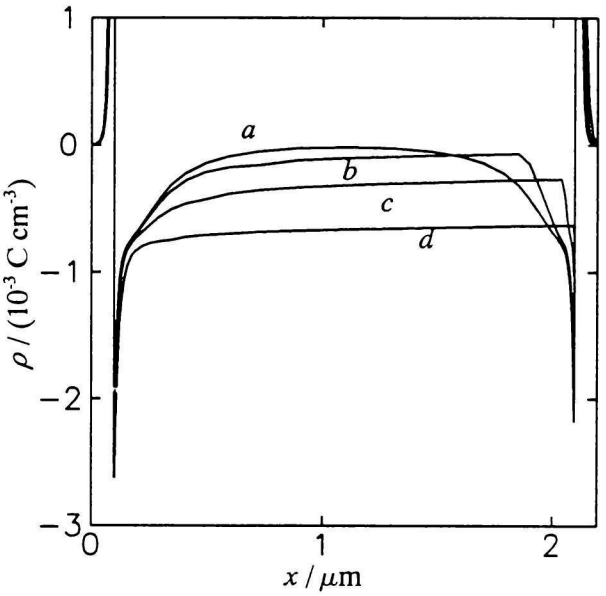

Fig. 15. Space-charge density spatial profiles along the n–i–n device under S-SCLC at zero bias (*a*) and at different applied voltages: $U = 1.1$ V (*b*), 4.8 V (*c*), 11.1 V (*d*).

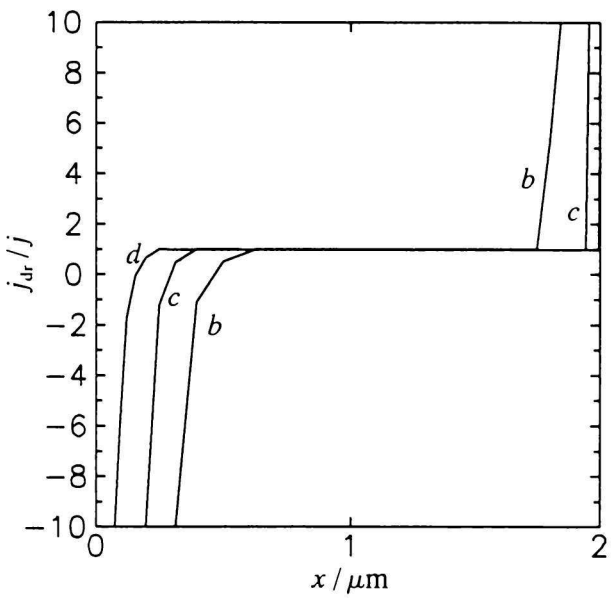

Fig. 16. The ratio of the drift to total current in the n–i–n device under S-SCLC corresponding to Figs. 14 and 15.

the curve *a*, where the structure is without the external applied voltage. The supposition about the infinite reservoir of charge carriers in the contact region (*i.e.* in the infinitely small region near $x = 0$) is hardly valid. This is more obvious in Fig. 15, where the spatial distribution of the space-charge density is presented for regimes identical to that in Fig. 14. Also the frequently expected flat band existence in the bulk of the material is not existent (at least for the sample thickness used here, *i.e.* $L = 2$ μm). So, the transition to SCLC regime is more gradual compared to the simple model represented by Stöckmann integrals and presented in the first part of the paper. As we increase the applied voltage (curves *b*—*d*), the transition to SCL current, represented by constant slope of the quasi-Fermi level, takes place (see curve *d*).

Also the frequently applied neglectance of the diffusion currents in SCLC was tested. We were able to calculate the value of the diffusion, drift and total currents for the systems in Figs. 14 and 15. The results are plotted in Fig. 16 as the ratio of the drift current j_{dr} over the total current $j = j_d + j_{dif}$. Again, we can see that the supposition about the small value of the diffusion component of the current in the whole sample is hardly acceptable, especially for low current densities. As the current increases (see curves *a* to *d*), the region with large diffusion currents diminishes. As a result of this time-consuming modelling we can obtain a measure for the necessary sample thickness to be able to extract correctly information presented in the first part of the paper. For the parameters chosen for modelling of Figs. 14—16 it was found that the necessary thickness for the method S-SCLC should not be less than $L = 5$ μm.

CONCLUSION

The present status of the method of space-charge-limited currents was presented, partially mirroring the results obtained in the laboratory of the authors. The main problems mastered by the theory of S-SCLC is possible to formulate:

1. The problem of the temperature-dependent SCLC, manifested by the complex dependence of the preexponential factor of SCL conductivity on its apparent, injection-dependent activation energy, was examined. Measuring on one sample and so changing the position of the quasi-Fermi level by injection only and not by the change of the density of localized states, we may in principle obtain more detailed information about the DOS distribution function. Starting from the theory of SCLC, we were able to derive the formula for the activation energy of SCL injection-dependent conductivity and to find its relation to the activation energy of the space-charge-free conductivity.

2. The limitation of the method, examined in the paper, is given by the "visibility" of the localized states with respect to the injected space charge which stems from the statistics of the occupation. The "visibility" of the localized states is given by the interplay of the crucial parameters describing the DOS function, *i.e.* its total concentration, energy position, and temperature. Generally one can say the shallower electronic state the lower temperature is necessary for the SCLC application to be spectroscopically effective.

3. The resolving power of the temperature-modulated space-charge-limited currents method especially in decreasing parts of the DOS functions was examined. This problem, occurring in real disordered semiconductors, has not been dealt with in the literature.

The description of this situation was limited to the so-called trap-filled limit (TFL) for the monoenergetic states, based on the fact of enormous move of the quasi-Fermi level on filling the monoenergetic state and corresponding steep increase of the current in the system, keeping the applied voltage virtually constant. We studied to what extent TFL range of SCLC data bears information on real decreasing DOS functions. We proved by numerical modelling that information on DOS is theoretically available and showed the limits of the evaluation, given by the mathematics involved. In real experiment the result of this part of SCLC characteristics is strongly dependent on precision of experimental data and this modelling experiment constitutes the upper achievable limit.

4. In the theory of S-SCLC of amphoteric defects we found that the filling of the amphoteric defects with the positive correlation energy $U > 0$ by SCLC injection takes place in *two separate successive steps* involving one electron each; the energy levels are situated in one electron representation at the energies E_t and $E_t + U$, each with the concentration N_t. The filling of the amphoteric defects with the negative correlation energy $U < 0$ by SCLC injection takes place in *one step* involving two electrons; the effective energy level is situated in one electron representation at the energy $E_t + U/2$, with the effective concentration $2N_t$. The transition from one-electron to two-electron filling of amphoteric defects with the negative correlation energy $U < 0$ may lead to the rise in the activation energy of the SCL current with the shift of the quasi-Fermi level and to an unexpected $j \approx V^{3/2}$ dependence of the current—voltage characteristic.

5. In this paper we also show that the one-carrier steady-state space-charge-limited currents can be used as a precise tool to study bulk energy distributions of trap levels in real systems provided that the structures with ohmic contacts or strongly doped contact layers are used to ensure the injection of one type of charged carriers into the intrinsic layer. Further, the influence of the finite temperature on the reconstructing of states broadening is examined. Every discrete trap level appears as a narrow energy distribution from the SCLC measurements.

REFERENCES

1. Lampert, M. A. and Mark, P., *Current Injection in Solids.* Academic Press, New York, 1970 and Kao, K. C. and Hwang, W., *Electrical Transport in Solids.* Pergamon Press, Oxford, 1981.
2. den Böer, W., *J. Phys.* (Paris) *42,* C4, 451 (1981).
3. Mackenzie, K. D., LeComber, P. G., and Spear, W. E., *Phil. Mag. 46,* 377 (1982).
4. Hassan, Y. M. and Wilson, J. B., *Solid State Commun. 49,* 771 (1984).
5. Chik, K. P., Yu, C. K., Lim, P. K., Tong, B. Y., John, P. K., and Wong, S. K., *Phys. Rev. B31,* 7827 (1985).
6. Gangopadhyay, S., Iselborn, S., Rübel, H., Schröder, B., and Geiger, J., *Phil. Mag. B51,* L38 (1985).
7. Nešpůrek, S., Zmeškal, O., and Schauer, F., *Phys. Status Solidi A 85,* 619 (1984).
8. Zmeškal, O., Schauer, F., and Nešpůrek, S., *J. Phys. C: Solid State Phys. 18,* 1873 (1985).
9. Schauer, F., Nešpůrek, S., and Zmeškal, O., *J. Phys. C: Solid State Phys. 19,* 7231 (1986).
10. Stöckmann, F., *Phys. Status Solidi A 64,* 475 (1981).
11. SNOVAL – Fortran program for the modelling of space charge-forming characteristics and TM-SCLC, available from the authors.
12. RECON – Pascal program for the evaluating of TM-SCLC characteristics, available from the authors.
13. Street, R. A. and Mott, N. F., *Phys. Rev. Lett. 35,* 1293 (1975).
14. Adler, D. and Yoffa, E. J., *Phys. Rev. Lett. 36,* 1197 (1976).
15. Okamoto, H. and Hamakawa, Y., *Solid State Commun. 24,* 23 (1977).
16. Schauer, F., Šmíd, V., and Žaludek, V., *Czech. J. Phys. B28,* 705 (1978).
17. Čech, V. and Schauer, F., in *Proc. 8th Int. School on Condensed Matter Physics: Electronic, Optoelectronic and Magnetic Thin Films, Varna, 1994.* (Marshall, J. M., Editor.) P. 620. Wiley, New York, 1995.

Translated by F. Schauer